ALS-associated mutant KIF5A forms oligomers and aggregates and induces neuronal toxicity

Juri Nakano[1,3], Kyoko Chiba[2,3,#] and Shinsuke Niwa[1,2,#]

1 Graduate school of Life Sciences, Tohoku University, Katahira 2-1, Aoba-ku, Sendai, Miyagi 980-8578, Japan

2 Frontier Research Institute for Interdisciplinary Sciences (FRIS), Tohoku University, Aramaki-Aoba 6-3, Aoba-ku, Sendai, Miyagi 980-0845, Japan

3 These authors equally contribute to this work

Corresponding authors

KYOKO CHIBA, Frontier Research Institute for Interdisciplinary Sciences (FRIS), Tohoku University, Aramaki-Aoba 6-3, Aoba-ku, Sendai, Miyagi 980-0845, Japan

e-mail: kyoko.chiba.e7@tohoku.ac.jp

SHINSUKE NIWA, Frontier Research Institute for Interdisciplinary Sciences (FRIS), Tohoku University, Aramaki-Aoba 6-3, Aoba-ku, Sendai, Miyagi 980-0845, Japan

e-mail: shinsuke.niwa.c8@tohoku.ac.jp

Author Contributions:

S.N. designed research; J.N., K.C., and S.N. performed research; J.N., K.C., and S.N analyzed data; J.N., K.C., and S.N. wrote the paper.

Competing Interest Statement:

The authors have no conflicts of interest directly relevant to the content of this article.

Keywords: KIF5A, ALS, aggregation

This PDF file includes:

Main Text

Figures 1 to 6

Abstract

KIF5A is a kinesin superfamily motor protein that transport various cargos in neurons. Mutations in *Kif5a* cause familial amyotrophic lateral sclerosis (ALS). These ALS mutations are in the intron of *Kif5a* and induce missplicing of KIF5A mRNA, leading to splicing out of exon 27. Exon 27 of KIF5A encodes a cargo-binding tail domain of KIF5A; therefore, it has been suggested ALS is caused by loss of function of KIF5A. However, precise mechanisms how mutations in KIF5A cause ALS remain to be clarified. Here, we show that the ALS-associated mutant of KIF5A, KIF5A(Δexon27), is predisposed to form oligomers and aggregations *in vivo* and *in vitro*. Interestingly, KIF5A(Δexon27) oligomers moved on microtubules more actively than wild type KIF5A *in vitro*. Moreover, KIF5A(Δexon27)-expressed worm neurons showed morphological defects. These data collectively suggest that ALS-associated mutations of KIF5A are toxic gain of function, rather than a simple loss of function.

Introduction

Neuronal development, function and maintenance depend on intracellular transport (Hirokawa, Noda, Tanaka, & Niwa, 2009). Kinesin superfamily proteins (KIFs) and cytoplasmic dyneins are molecular motors for anterograde and retrograde transport, respectively (Hirokawa, Niwa, & Tanaka, 2010; Kardon & Vale, 2009). Among KIFs, Kinesin-1, -2 and -3 family members are main anterograde transporters in the neuron (Hall & Hedgecock, 1991; Iwata, Morikawa, Takei, & Hirokawa, 2020; Niwa, Tanaka, & Hirokawa, 2008 ; Okada, Yamazaki, Sekine-Aizawa, & Hirokawa, 1995; Scholey, 2008; Tanaka et al., 1998; Uchida, Alami, & Brown, 2009 ; Vale, Reese, & Sheetz, 1985; Xia et al., 2003). KIFs generally consist of a conserved motor domain, coiled-coil domains to dimerize and a cargo-binding tail domain. The motor domain has a microtubule-stimulated ATPase activity to move on microtubules (Hackney, 1995). Each KIF has a diversified tail domain (Vale, 2003). The tail domain binds to cargo vesicles and protein complexes (Hirokawa et al., 2009).

Advances in the genomic sequence technology have identified many diseases associated mutations in motor protein genes (Hirokawa et al., 2010; Holzbaur & Scherer, 2011) . Mutations in KIFs and dynein subunits often cause motor neuron diseases. Mutations in Kinesin-3, such as KIF1A and KIF1B, cause hereditary spastic paraplegia and Charcot-Marie-Tooth type 2A1 (Boyle et al., 2021; Budaitis et al., 2021; Chiba et al., 2019 ; Zhao et al., 2001). Mutations in dynein heavy chain 1 (DYNC1H1) are causes of CMT type 2O and spinal muscular atrophy-1 (SMA) (Harms et al., 2012; Weedon et al., 2011). Mutations in p150 subunit of dynactin (DCTN1), an activator for dynein, cause ALS (Munch et al., 2004). Gain of function mutations in BICD2, cargo adaptor protein for cytoplasmic dynein complex, are causes of spinal muscular atrophy (Huynh & Vale, 2017). Mutations in KIF5A are associated with hereditary spastic paraplegia (SPG) and ALS (D. Brenner et al., 2018; Nicolas et al., 2018; Reid et al., 2002). Mutated residues are different in KIF5A-associated SPG and ALS. SPG is caused by motor domain mutations in KIF5A. These

mutations abolish the motor activity of KIF5A motor (Ebbing et al., 2008). On the other hand, ALS-associated KIF5A mutations commonly induce missplicing and a deletion of exon 27 (Fig 1A) (D. Brenner et al., 2018; Nicolas et al., 2018). Previous studies have suggested ALS mutations in KIF5A are loss-of-function due to the deletion of the cargo-binding tail domain (D. Brenner et al., 2018; Nicolas et al., 2018). However, the precise molecular mechanism of KIF5A-associated ALS has not been shown.

We show here that the product of ALS-associated KIF5A alleles, KIF5A(Δexon27), is predisposed to form oligomers and aggregations. The binding of KLC1, one of the cargo adaptors for KIF5A, was not affected by Δexon27. Interestingly, KIF5A(Δexon27) oligomers showed higher motility than wild type KIF5A regardless of the presence of KLC1. Exogenous expression of KIF5A(Δexon27) caused defects in neuronal morphology in *C. elegans*. Taken together, we suggest ALS-associated mutations in KIF5A are toxic gain of function, rather than a simple loss of function mutation.

Results

KIF5A(Δexon27) form aggregations in the cell

To study the molecular mechanism of ALS caused by KIF5A mutations, we expressed mScarlet fused KIF5A (mSca::KIF5A) and mScarlet fused KIF5A(Δexon27) (mSca::KIF5A(Δexon27)) in a neuron-like cell line CAD (Qi, Wang, McMillian, & Chikaraishi, 1997) (Fig 1B-E). mSca::KIF5A was mostly diffuse in the cell but about 30 % mSca::KIF5A-expressed cells showed small aggregates in the cytoplasm (Fig 1C and E) in agreement with our prior finding showing a propensity of KIF5A to form oligomers (Chiba, Ori-McKenney, Niwa, & McKenney, 2022). The ratio of cells showing aggregation is higher compared with cells expressing mScarlet fused KIF5B, a homologue of KIF5A (Hirokawa et al., 2009). Only 10% of mSca::KIF5B-expressed cells showed aggregations. In contrast, in 97 % cells, mSca::KIF5A(Δexon27) formed many aggregates in the

cytoplasm. We found aggregates often accumulate to the tip of neurites in CAD cells (Fig 1D arrows), which is similar to the localization of KIF5A with constitutive-active mutations (Nakata, Niwa, Okada, Perez, & Hirokawa, 2011). Almost no aggregates were found in mScarlet-expressing cells (Fig 1E). These data suggest that KIF5A tends to form aggregates in the cell and the ALS-associated mutation, Δexon27, strongly enhances the formation of aggregates.

KIF5A(Δexon27) co-aggregates with wild type motors

We asked whether the ALS-associated KIF5A protein co-aggregates with wild type motors. mSca::KIF5A(Δexon27) was co-expressed with enhanced green fluorescent protein (EGFP)-labelled KIF5A (EGFP::KIF5A). Previous studies have shown that KIF5A forms a homodimer to move on microtubules (Hackney, 1995; Hackney, Levitt, & Wagner, 1991; Vale et al., 1996). As anticipated from this notion, mSca::KIF5A(Δexon27) co-aggregates with EGFP::KIF5A(wt) in the cell (Fig 2A-D). Aggregates were accumulated to tips of CAD cell neurites. *Homo sapiens* have three homologous kinesin heavy chain genes: KIF5A, KIF5B and KIF5C (Hirokawa et al., 2009). Three proteins are highly conserved, but they do not form heterodimers (Kanai et al., 2000). Interestingly, mSca::KIF5A(Δexon27) co-aggregtated with EGFP::KIF5B(wt) (Fig. 2E-H). While EGFP::KIF5B was diffuse in the cytoplasm when mSca::KIF5A did not form aggregates (Fig 2E and F), EGFP::KIF5B(wt) was mis-accumulated to neurite tips and co-aggregated with mSca::KIF5A(Δexon27) (Fig 2G and H). In contrast, mSca::KIF5A(Δexon27) did not co-aggregate with EGFP (Fig 2I and J). These data suggest that KIF5A(Δexon27) co-aggregates with wild type KIF5A and KIF5B motors in the cell.

KIF5A(Δexon27) oligomerizes *in vitro*

Kinesin-1 is a heterotetramer composed of two heavy chains (KIF5) and two light chains (KLC)

(Hackney et al., 1991). We have previously shown that KIF5A has a propensity to form oligomers *in vitro* (Chiba et al., 2022). To examine the effect of Δexon27 mutation on the interaction with KLC1 and oligomerization, we next purified heavy chain dimers (KIF5A) and Kinesin-1 tetramers (KIF5A-KLC1) in the presence or absence of Δexon27 mutation. Firstly, we expressed full-length KIF5A::mSca and KIF5A(Δexon27)::mSca in sf9 cells and purified them by affinity chromatography and size exclusion chromatography (SEC) (Chiba et al., 2022). In the SEC, wild type KIF5A predominantly eluted in a single peak (Fig 3A, blue shaded area). In addition, small amount of wild type KIF5A was recovered from earlier fractions than the major peak and from the void volume (Fig 3A, red shaded area and yellow shaded area). We have shown that the main peak corresponds to KIF5A dimers and the minor peak eluded earlier than the main peak represent KIF5A oligomers (Chiba et al., 2022). Next, we tested KIF5A(Δexon27) and found that Δexon27 mutation dramatically changes the elution profile from wild type KIF5A. The major elution peak of Δexon27 shifted towards a higher molecular weight which corresponds to oligomers (Fig 3A, red shaded area). Most of KIF5A(Δexon27) was recovered from higher molecular weight fractions but not from dimer fractions. Thus, Δexon27 mutation induces oligomerization of KIF5A. We note that Δexon27 also increased the population recovered from the void volume, suggesting a potential of KIF5A(Δexon27) to form aggregates as well as oligomers (Fig 3A, yellow shaded area).

Next, to test whether the binding of kinesin light chain (KLC) subunit is affected or not, we co-expressed KLC1 with full length KIF5A or KIF5A(Δexon27). KLC1 was co-purified either with KIF5A(wt) or KIF5A(Δexon27) (Fig 3B and 3C). The ratio between heavy chains and light chains was almost 1:1 and was not strongly affected by Δexon27. Thus, the binding with KLC is not abolished by the deletion of exon 27. KIF5A-KLC1 complex showed a similar elution profile as KIF5A in the SEC analysis (Fig 3B, blue lines). Whith KIF5A(Δexon27)-KLC1, we again observed a peak shifted towards a higher molecular weight and increased population recovered from the void

volume. These results suggest that the propensity of KIF5A(Δexon27) to form oligomers and aggregates is not largely affected by KLC1.

KIF5A(Δexon27) oligomers are hyperactivated on microtubules

We analyzed the motility of the purified motors on microtubules at the single molecule resolution by total internal reflection fluorescence (TIRF) microscopy (Chiba et al., 2022; Chiba et al., 2019; McKenney, Huynh, Tanenbaum, Bhabha, & Vale, 2014). Purified full-length KIF5A(wt)::mSca and KIF5A(wt)::mSca-KLC1 did not bind nor move well on microtubules (Fig 4A and 4B). This is because of the autoinhibitory mechanism described previously (Coy, Hancock, Wagenbach, & Howard, 1999; Friedman & Vale, 1999) (Chiba et al., 2022). In contrast, we found full-length KIF5A(Δexon27)::mSca and full-length KIF5A(Δexon27)::mSca-KLC1 frequently bound to microtubules and moved (Fig 4A-C). In average, the binding rate of KIF5A(Δexon27)::mSca and KIF5A(Δexon27)::mSca-KLC1 were 9-times higher than KIF5A(wt)::mSca and KIF5A(wt)::mSca-KLC1, respectively (Fig 4C). The run length of KIF5A(Δexon27)::mSca and KIF5A(Δexon27)::mSca-KLC1 was much longer than wild type KIF5A (~ 1 μm) (Chiba et al., 2022) . While the run length of wild type proteins could not be measured in this condition, the median value of the run length of KIF5A(Δexon27)::mSca and KIF5A(Δexon27)::mSca-KLC1 were approximately 3 μm (Fig 4D). No significant difference was detected between KIF5A(Δexon27)::mSca and KIF5A(Δexon27)::mSca-KLC1. The velocity of KIF5A(Δexon27)::mSca and KIF5A(Δexon27)::mSca-KLC1 was comparable (Fig 4E and F). Taken together, KIF5A oligomers induced by Δexon27 are more active than wild type KIF5A both in the presence or absence of KLC subunit.

KIF5A(Δexon27) oligomers tend to form aggregations

To test the property of KIF5A(Δexon27), we incubated purified KIF5A(Δexon27) at 37°C and measured the turbidity of protein solutions by the optical density at 600 nm (OD_{600}). It has been shown that formation of protein aggregates in solution can be monitored by OD_{600} (Schafheimer & King, 2013). Immediately before the incubation, protein solutions were centrifuged and clarified. The turbidity of purified mSca::KIF5A(Δexon27) increased gradually (Fig 4A). 24 hours later, the solution was again centrifuged. Purified mSca::KIF5A(Δexon27) showed a protein pellet (Fig 4B). Purified mScarlet did not form aggregations at all even after the 24-hour incubation. These data indicate that KIF5A(Δexon27) tend to form protein aggregates in vitro.

KIF5A(Δexon27) is toxic in C. elegans neurons

Previous studies have shown that ALS is caused by toxic gain of function mutations (Johnson et al., 2009) (Bruijn et al., 1998) (Kwiatkowski et al., 2009). Then, we tested the toxicity of KIF5A(Δexon27) in *C. elegans* neurons. The morphology of mechanosensory neurons were compared by expressing human KIF5A and KIF5A(Δexon27) (Fig 6A-F). Mechanosensory neurons were analyzed because many studies have shown that these neurons have very stereotypical morphology and show very small variations in the *wild type* background (Gallegos & Bargmann, 2004; Ghosh-Roy, Goncharov, Jin, & Chisholm, 2012). At day 1 adults, the morphology of PLM and PVM neurons were observed and compared. PLM neuron had a long straight axon along the body in the *wild type* (Fig 6A and B). In KIF5A-expressed neurons, no significant differences were found compared with control neurons (Fig 6C). In contrast, KIF5A(Δexon27)-expressed neurons showed morphological defects (Fig 6D-F). About 60% worms showed abnormal PLM and PVM morphologies (Fig 6D). No stereotypical abnormalities were found. PLM cell body was often mislocalized. Some worms had PLM neuron with multiple neuronal processes. Other worms had PLM neurons that have bent axons. About 20 % worms showed neuronal loss (Fig 6E). These data

suggest that KIF5A(Dexon27) has toxicity in neurons.

Discussion

Previous studies have suggested that KIF5A(Δexon27) causes ALS by a loss-of-function mechanism because the cargo binding tail domain is deleted (D. Brenner et al., 2018; Nicolas et al., 2018). However, while several loss-of-function mutations have been found in the motor domain of KIF5A, these mutations cause hereditary spastic paraplegia, rather than ALS (Ebbing et al., 2008; Reid et al., 2002). None of motor domain mutations in KIF5A have been associated with ALS. These genetic data suggest ALS mutations in KIF5A are not simple loss-of-function. Protein aggregations are often associated with neurodegenerative disorders (Soto, 2003). A lot of ALS-associated mutations have been identified in other genes such as TARDBP (TDP-43 gene), SOD and FUS (Aoki et al., 1993; Kabashi et al., 2008; Kwiatkowski et al., 2009; Vance et al., 2009). These mutations commonly induce aggregates that are toxic in cells (Johnson et al., 2009) (Bruijn et al., 1998) (Kwiatkowski et al., 2009). Our data suggest Δexon27 mutation in KIF5A induces toxic aggregations. While we are preparing this manuscript, a preprint showing similar results has been posted on Biorxiv (Pant et al., 2022). They show unpurified KIF5A(Δexon27) in cell lysates is more active than wild type KIF5A; however, it remained elusive KIF5A(Δexon27) by itself is hyperactive or KIF5A(Δexon27) is activated by binding with unidentified factors. Moreover, it remained elusive whether KIF5A(Δexon27) by itself form aggregates or the abnormal tail domain caused by frameshift binds to other factors that induce aggregates. Our assays using purified proteins support KIF5A(Δexon27) is hyperactive and is predisposed to form aggregates without the involvement of other factors. How is the hyperactivation of KIF5A motor related to toxicity in neurons? One possibility is that hyperactivation of KIF5A causes mis-accumulation of KIF5A at axonal tips, leading to highly concentrated KIF5A and enhancement of aggregate formation. This hypothesis is

supported by the observation that KIF5(Δexon27) aggregates are often observed at neurite tips in CAD cells (Fig 1). Another possibility is that hyperactivated KIF5A changes the distribution of cargo organelles and induce cellular toxicity. Further analyses will be needed to test whether ALS-associated KIF5A changes the localization of organelles.

We have previously shown KIF5A forms more oligomers than KIF5B and KIF5C *in vitro* (Chiba et al., 2022). KIF5A oligomers are more active than KIF5A dimers. The physiological significance of this phenomena remains to be elusive. We show here even wild type KIF5A has a propensity to form more aggregates in the cell, compared with KIF5B (Fig 1). Similar property has been found in TDP-43. TDP-43 is intrinsically aggregation-prone, which implies TPD-43 may be directly involved in the pathogenesis of sporadic ALS (Johnson et al., 2009). It is possible that the oligomerize-prone property of KIF5A is related to sporadic ALS and the property is enhanced by ALS-associated KIF5A mutations.

Experimental Procedures

Molecular biology

Polymerase chain reaction (PCR) was performed using KOD FX neo (TOYOBO, Tokyo, Japan) as described in the manual. Restriction enzymes were purchased from New England BioLabs Japan (Tokyo, Japan).

pAcebac1 plasmids containing human *KIF5A*(BC146670) human *KIF5B*(BC126281), and *KLC1* (BC008881) was described previously (Chiba et al., 2022).

To generate mScarlet::KIF5A and mScarlet::KIF5B expressing plasmids, pmScarletC1 plasmid was obtained from Addgene. KIF5A and KIF5B were amplified by PCR and transferred to pmScarletC1. To generate an EGFP::KIF5B expressing vector, EGFP was amplified from pEGFPN1::KIF1A (Niwa et al., 2008) and replaced with mScarlet by using AgeI and XhoI sites.

Δexon27 mutation was introduced by Gibson assembly. cDNA fragment encoding the mutated domain (Fig 1A) was synthesized by gBlocks (Integrated DNA Technologies Japan, Tokyo, Japan) and replated with the wild-type fragment by Gibson assembly (Gibson et al., 2009). Plasmids used in this paper is described in ***supplementary table S1***.

CAD cell experiments

CAD cells were obtained from European Collection of Cell Cultures (Salisbury, UK) and maintained as described (Qi et al., 1997). For observation, cells were cultured on glass coverslips (Matsunami, Tokyo, Japan). Plasmid transfection was performed by Lipofectamine LTX (Thermo Fisher Scientific) as described in the manufacturer's manual. 24 hours after the transfection, mScarlet and GFP signals were observed under Zeiss Axio Observer inverted microscope equipped with LSM800 confocal unit (Carl Zeiss). x40 water immersion objective lens (Numerical Aperture: 1.1) was used for imaging. ZEN software (Carl Zeiss) was used to control the system.

Purification of KIF5A

pAcebac plasmids were transformed to generate bacmid. Sf9 cells were maintained as a suspension culture in Sf-900II serum-free medium (SFM) (Thermo Fisher Scientific) at 27°C. To prepare baculovirus, 1 x 10^6 cells of Sf9 cells were transferred to each well of a tissue-culture treated 6 well plate. After the cells attached to the bottom of the dishes, about ~5 µg of bacmid were transfected using 6 µl of Cellfectin II reagent (Thermo Fisher Scientific). 5 days after initial transfection, the culture media were collected and spun at 3000 x g for 3 min to obtain the supernatant (P1). For protein expression, 400 ml of Sf9 cells (2 x 10^6 cells/ml) were infected with 100 µl of P1 virus and cultured for 65 hr at 27°C. Cells were harvested and resuspended in 25 ml of lysis buffer (50 mM HEPES-KOH, pH 7.5, 150 mM KCH_3COO, 2 mM MgSO4, 1 mM EGTA, 10%

glycerol) along with 1 mM DTT, 1 mM PMSF, 0.1 mM ATP and 0.5% TritonX-100. After incubating on ice for 10 min, the lysates were centrifuged at 15000 x g for 20 min at 4°C. The resulting supernatant were subject to affinity chromatography described below.

For affinity chromatography, the supernatants were put over a column of Streptactin XT resin (IBA) at 4°C. The columns were then washed with excess lysis buffer to remove unbound material and the proteins were eluted in lysis buffer containing 100 mM D-biotin. Eluted proteins were further purified via size exclusion chromatography using a Superose 6 10/300 GL column (Cytiva) equilibrated in lysis buffer. Fractions containing the proteins were combined and concentrated on amicon spin filters with a 50 kDa cutoff. Concentrated proteins were frozen in LiN_2 and stored at -80°C.

TIRF single-molecule motility assays

TIRF assays were performed as described (Chiba et al., 2019). Tubulin was purified from porcine brain as described (Castoldi & Popov, 2003). Tubulin was labeled with Biotin-PEG_2-NHS ester (Tokyo Chemical Industry, Tokyo, Japan) and AZDye647 NHS ester (Fluoroprobes, Scottsdale, AZ, USA) as described (Al-Bassam, 2014). To polymerize Taxol-stabilized microtubules labeled with biotin and AZDye647, 30 μM unlabeled tubulin, 1.5 μM biotin-labeled tubulin and 1.5 μM AZDye647-labeled tubulin were mixed in BRB80 buffer supplemented with 1 mM GTP and incubated for 15 min at 37°C. Then, an equal amount of BRB80 supplemented with 40 μM taxol was added and further incubated for more than 15 min. The solution was loaded on BRB80 supplemented with 300 mM sucrose and 20 μM taxol and ultracentrifuged at 100,000 g for 5 min at 30°C. The pellet was resuspended in BRB80 supplemented with 20 μM taxol. Glass chambers were prepared by acid washing as previously described (McKenney et al., 2014). Glass chambers were coated with PLL-PEG-biotin (SuSoS, Dübendorf, Switzerland). Polymerized microtubules were flowed into

streptavidin adsorbed flow chambers and allowed to adhere for 5–10 min. Unbound microtubules were washed away using assay buffer [90 mM Hepes pH 7.4, 50 mM KCH_3COO, 2 mM $Mg(CH_3COO)_2$, 1 mM EGTA, 10% glycerol, 0.1 mg/ml biotin–BSA, 0.2 mg/ml kappa-casein, 0.5% Pluronic F127, 2 mM ATP, and an oxygen scavenging system composed of PCA/PCD/Trolox. Purified motor protein was diluted to indicated concentrations in the assay buffer. Then, the solution was flowed into the glass chamber. An ECLIPSE Ti2-E microscope equipped with a CFI Apochromat TIRF 100XC Oil objective lens, an Andor iXion life 897 camera and a Ti2-LAPP illumination system (Nikon, Tokyo, Japan) was used to observe single molecule motility. NIS-Elements AR software ver. 5.2 (Nikon) was used to control the system.

Worm experiments and strains

C. elegans strains were maintained as described previously (S. Brenner, 1974). Wild-type worm N2 and feeder bacteria OP50 were obtained from C. elegans genetic center (CGC) (Minneapolis, MN, USA). Nematode Growth Media (NGM) agar plates were prepared as described (S. Brenner, 1974). Transformation of C. elegans was performed by DNA injection as described (Mello, Kramer, Stinchcomb, & Ambros, 1991).

Strains used in this study are described in supplementary table S2.

Analysis of mechanosensory neurons in C. elegans

Mechanosensory neurons were visualized using *uIs31* [*Pmec-7::gfp*] marker that was obtained from *C. elegans* genetic center (Minnesota, USA) (Chalfie, Tu, Euskirchen, Ward, & Prasher, 1994). Strains expressing human KIF5A or KIF5A(Δexon27) were observed under Zeiss Axio Observer inverted microscope equipped with LSM800 confocal unit (Carl Zeiss, Jena, Germany). x20 objective lens (Numerical Aperture: 0.8) was used for imaging. ZEN software (Carl

Zeiss) was used to control the system. Fiji was used to analyze image files (Schindelin et al., 2012).

Acknowledgements

We thank all the members of McKenney lab (UC Davis), Sugimoto lab (Tohoku Univ.) and Niwa lab (Tohoku Univ.) for helpful discussion. SN was supported by JSPS KAKENHI (20H03247, 19H04738, 20K21378), the Kato Memorial Bioscience Foundation and Takeda Science Foundation. KC was supported by JSPS KAKENHI (21K20621) and MEXT Leading Initiative for Excellent Researchers. Some worm strains and OP50 were obtained from the CGC.

Al-Bassam, J. (2014). Reconstituting Dynamic Microtubule Polymerization Regulation by TOG Domain Proteins. *Methods in Enzymology, 540*, 131-148. doi:10.1016/B978-0-12-397924-7.00008-X

Aoki, M., Ogasawara, M., Matsubara, Y., Narisawa, K., Nakamura, S., Itoyama, Y., & Abe, K. (1993). Mild ALS in Japan associated with novel SOD mutation. *Nat Genet, 5*(4), 323-324. doi:10.1038/ng1293-323

Boyle, L., Rao, L., Kaur, S., Fan, X., Mebane, C., Hamm, L., . . . Chung, W. K. (2021). Genotype and defects in microtubule-based motility correlate with clinical severity in KIF1A-associated neurological disorder. *HGG Adv, 2*(2). doi:10.1016/j.xhgg.2021.100026

Brenner, D., Yilmaz, R., Muller, K., Grehl, T., Petri, S., Meyer, T., . . . German, A. L. S. n. M. N. D. N. E. T. (2018). Hot-spot KIF5A mutations cause familial ALS. *Brain, 141*(3), 688-697. doi:10.1093/brain/awx370

Brenner, S. (1974). The genetics of Caenorhabditis elegans. *Genetics, 77*(1), 71-94. Retrieved from https://www.ncbi.nlm.nih.gov/pubmed/4366476

Bruijn, L. I., Houseweart, M. K., Kato, S., Anderson, K. L., Anderson, S. D., Ohama, E., . . . Cleveland, D. W. (1998). Aggregation and motor neuron toxicity of an ALS-linked SOD1 mutant independent from wild-type SOD1. *Science, 281*(5384), 1851-1854. doi:10.1126/science.281.5384.1851

Budaitis, B. G., Jariwala, S., Rao, L., Yue, Y., Sept, D., Verhey, K. J., & Gennerich, A. (2021). Pathogenic mutations in the kinesin-3 motor KIF1A diminish force generation and movement through allosteric mechanisms. *J Cell Biol, 220*(4). doi:10.1083/jcb.202004227

Castoldi, M., & Popov, A. V. (2003). Purification of brain tubulin through two cycles of polymerization-depolymerization in a high-molarity buffer. *Protein Expr Purif, 32*(1), 83-88. doi:10.1016/S1046-5928(03)00218-3

Chalfie, M., Tu, Y., Euskirchen, G., Ward, W. W., & Prasher, D. C. (1994). Green fluorescent protein as a

marker for gene expression. *Science, 263*(5148), 802-805. doi:10.1126/science.8303295

Chiba, K., Ori-McKenney, K. M., Niwa, S., & McKenney, R. J. (2022). Reconstitution of a Synergistic Kinesin-1 Activation Mechanism. *Cell Rep, in press*.

Chiba, K., Takahashi, H., Chen, M., Obinata, H., Arai, S., Hashimoto, K., . . . Niwa, S. (2019). Disease-associated mutations hyperactivate KIF1A motility and anterograde axonal transport of synaptic vesicle precursors. *Proc Natl Acad Sci U S A, 116*(37), 18429-18434. doi:10.1073/pnas.1905690116

Coy, D. L., Hancock, W. O., Wagenbach, M., & Howard, J. (1999). Kinesin's tail domain is an inhibitory regulator of the motor domain. *Nat Cell Biol, 1*(5), 288-292. doi:10.1038/13001

Ebbing, B., Mann, K., Starosta, A., Jaud, J., Schols, L., Schule, R., & Woehlke, G. (2008). Effect of spastic paraplegia mutations in KIF5A kinesin on transport activity. *Hum Mol Genet, 17*(9), 1245-1252. doi:10.1093/hmg/ddn014

Friedman, D. S., & Vale, R. D. (1999). Single-molecule analysis of kinesin motility reveals regulation by the cargo-binding tail domain. *Nat Cell Biol, 1*(5), 293-297. doi:10.1038/13008

Gallegos, M. E., & Bargmann, C. I. (2004). Mechanosensory neurite termination and tiling depend on SAX-2 and the SAX-1 kinase. *Neuron, 44*(2), 239-249. doi:10.1016/j.neuron.2004.09.021

Ghosh-Roy, A., Goncharov, A., Jin, Y., & Chisholm, A. D. (2012). Kinesin-13 and tubulin posttranslational modifications regulate microtubule growth in axon regeneration. *Dev Cell, 23*(4), 716-728. doi:10.1016/j.devcel.2012.08.010

Gibson, D. G., Young, L., Chuang, R. Y., Venter, J. C., Hutchison, C. A., 3rd, & Smith, H. O. (2009). Enzymatic assembly of DNA molecules up to several hundred kilobases. *Nat Methods, 6*(5), 343-345. doi:10.1038/nmeth.1318

Hackney, D. D. (1995). Highly processive microtubule-stimulated ATP hydrolysis by dimeric kinesin head domains. *Nature, 377*(6548), 448-450. doi:10.1038/377448a0

Hackney, D. D., Levitt, J. D., & Wagner, D. D. (1991). Characterization of alpha 2 beta 2 and alpha 2 forms of kinesin. *Biochem Biophys Res Commun, 174*(2), 810-815. Retrieved from https://www.ncbi.nlm.nih.gov/pubmed/1825168

Hall, D. H., & Hedgecock, E. M. (1991). Kinesin-related gene unc-104 is required for axonal transport of synaptic vesicles in C. elegans. *Cell, 65*(5), 837-847. Retrieved from https://www.ncbi.nlm.nih.gov/pubmed/1710172

Harms, M. B., Ori-McKenney, K. M., Scoto, M., Tuck, E. P., Bell, S., Ma, D., . . . Baloh, R. H. (2012). Mutations in the tail domain of DYNC1H1 cause dominant spinal muscular atrophy. *Neurology, 78*(22), 1714-1720. doi:10.1212/WNL.0b013e3182556c05

Hirokawa, N., Niwa, S., & Tanaka, Y. (2010). Molecular motors in neurons: transport mechanisms and roles in brain function, development, and disease. *Neuron, 68*(4), 610-638. doi:10.1016/j.neuron.2010.09.039

Hirokawa, N., Noda, Y., Tanaka, Y., & Niwa, S. (2009). Kinesin superfamily motor proteins and intracellular transport. *Nat Rev Mol Cell Biol, 10*(10), 682-696. doi:10.1038/nrm2774

Holzbaur, E. L., & Scherer, S. S. (2011). Microtubules, axonal transport, and neuropathy. *N Engl J Med, 365*(24), 2330-2332. doi:10.1056/NEJMcibr1112481

Huynh, W., & Vale, R. D. (2017). Disease-associated mutations in human BICD2 hyperactivate motility of dynein-dynactin. *Journal of Cell Biology, 216*(10), 3051-3060. doi:10.1083/jcb.201703201

Iwata, S., Morikawa, M., Takei, Y., & Hirokawa, N. (2020). An activity-dependent local transport regulation via degradation and synthesis of KIF17 underlying cognitive flexibility. *Sci Adv, 6*(51). doi:10.1126/sciadv.abc8355

Johnson, B. S., Snead, D., Lee, J. J., McCaffery, J. M., Shorter, J., & Gitler, A. D. (2009). TDP-43 is intrinsically aggregation-prone, and amyotrophic lateral sclerosis-linked mutations accelerate aggregation and increase toxicity. *J Biol Chem, 284*(30), 20329-20339. doi:10.1074/jbc.M109.010264

Kabashi, E., Valdmanis, P. N., Dion, P., Spiegelman, D., McConkey, B. J., Vande Velde, C., . . . Rouleau, G. A. (2008). TARDBP mutations in individuals with sporadic and familial amyotrophic lateral sclerosis. *Nat Genet, 40*(5), 572-574. doi:10.1038/ng.132

Kanai, Y., Okada, Y., Tanaka, Y., Harada, A., Terada, S., & Hirokawa, N. (2000). KIF5C, a novel neuronal kinesin enriched in motor neurons. *J Neurosci, 20*(17), 6374-6384. Retrieved from https://www.ncbi.nlm.nih.gov/pubmed/10964943

Kardon, J. R., & Vale, R. D. (2009). Regulators of the cytoplasmic dynein motor. *Nat Rev Mol Cell Biol, 10*(12), 854-865. doi:10.1038/nrm2804

Kwiatkowski, T. J., Jr., Bosco, D. A., Leclerc, A. L., Tamrazian, E., Vanderburg, C. R., Russ, C., . . . Brown, R. H., Jr. (2009). Mutations in the FUS/TLS gene on chromosome 16 cause familial amyotrophic lateral sclerosis. *Science, 323*(5918), 1205-1208. doi:10.1126/science.1166066

McKenney, R. J., Huynh, W., Tanenbaum, M. E., Bhabha, G., & Vale, R. D. (2014). Activation of cytoplasmic dynein motility by dynactin-cargo adapter complexes. *Science, 345*(6194), 337-341. doi:10.1126/science.1254198

Mello, C. C., Kramer, J. M., Stinchcomb, D., & Ambros, V. (1991). Efficient gene transfer in C.elegans: extrachromosomal maintenance and integration of transforming sequences. *EMBO J, 10*(12), 3959-3970. Retrieved from https://www.ncbi.nlm.nih.gov/pubmed/1935914

Munch, C., Sedlmeier, R., Meyer, T., Homberg, V., Sperfeld, A. D., Kurt, A., . . . Ludolph, A. C. (2004). Point mutations of the p150 subunit of dynactin (DCTN1) gene in ALS. *Neurology, 63*(4), 724-726. doi:10.1212/01.wnl.0000134608.83927.b1

Nakata, T., Niwa, S., Okada, Y., Perez, F., & Hirokawa, N. (2011). Preferential binding of a kinesin-1 motor to GTP-tubulin-rich microtubules underlies polarized vesicle transport. *J Cell Biol, 194*(2), 245-255. doi:10.1083/jcb.201104034

Nicolas, A., Kenna, K. P., Renton, A. E., Ticozzi, N., Faghri, F., Chia, R., . . . Landers, J. E. (2018). Genome-wide Analyses Identify KIF5A as a Novel ALS Gene. *Neuron, 97*(6), 1268-1283 e1266. doi:10.1016/j.neuron.2018.02.027

Niwa, S., Tanaka, Y., & Hirokawa, N. (2008). KIF1Bbeta- and KIF1A-mediated axonal transport of presynaptic regulator Rab3 occurs in a GTP-dependent manner through DENN/MADD. *Nat Cell Biol, 10*(11), 1269-1279. doi:10.1038/ncb1785

Okada, Y., Yamazaki, H., Sekine-Aizawa, Y., & Hirokawa, N. (1995). The neuron-specific kinesin superfamily protein KIF1A is a unique monomeric motor for anterograde axonal transport of synaptic vesicle precursors. *Cell, 81*(5), 769-780. Retrieved from https://www.ncbi.nlm.nih.gov/pubmed/7539720

Pant, C. D., Parameswarn, J., Rao, L., Shi, L., Chilukuri, G., McEachin, T. Z., . . . Jiang, J. (2022). ALS-linked KIF5A ΔExon27 mutant causes neuronal toxicity through gain of function. *Biorxiv*. doi:10.1101/2022.03.05.483071

Qi, Y., Wang, J. K., McMillian, M., & Chikaraishi, D. M. (1997). Characterization of a CNS cell line, CAD, in which morphological differentiation is initiated by serum deprivation. *J Neurosci, 17*(4), 1217-1225. Retrieved from https://www.ncbi.nlm.nih.gov/pubmed/9006967

Reid, E., Kloos, M., Ashley-Koch, A., Hughes, L., Bevan, S., Svenson, I. K., . . . Marchuk, D. A. (2002). A kinesin heavy chain (KIF5A) mutation in hereditary spastic paraplegia (SPG10). *Am J Hum Genet, 71*(5), 1189-1194. doi:10.1086/344210

Schafheimer, N., & King, J. (2013). Tryptophan cluster protects human gammaD-crystallin from ultraviolet radiation-induced photoaggregation in vitro. *Photochem Photobiol, 89*(5), 1106-1115. doi:10.1111/php.12096

Schindelin, J., Arganda-Carreras, I., Frise, E., Kaynig, V., Longair, M., Pietzsch, T., . . . Cardona, A. (2012). Fiji: an open-source platform for biological-image analysis. *Nat Methods, 9*(7), 676-682. doi:10.1038/nmeth.2019

Scholey, J. M. (2008). Intraflagellar transport motors in cilia: moving along the cell's antenna. *J Cell Biol, 180*(1), 23-29. doi:10.1083/jcb.200709133

Soto, C. (2003). Unfolding the role of protein misfolding in neurodegenerative diseases. *Nat Rev Neurosci, 4*(1), 49-60. doi:10.1038/nrn1007

Tanaka, Y., Kanai, Y., Okada, Y., Nonaka, S., Takeda, S., Harada, A., & Hirokawa, N. (1998). Targeted disruption of mouse conventional kinesin heavy chain, kif5B, results in abnormal perinuclear clustering of mitochondria. *Cell, 93*(7), 1147-1158. doi:10.1016/s0092-8674(00)81459-2

Uchida, A., Alami, N. H., & Brown, A. (2009). Tight functional coupling of kinesin-1A and dynein motors in the bidirectional transport of neurofilaments. *Mol Biol Cell, 20*(23), 4997-5006. doi:10.1091/mbc.E09-04-0304

Vale, R. D. (2003). The molecular motor toolbox for intracellular transport. *Cell, 112*(4), 467-480.

Retrieved from https://www.ncbi.nlm.nih.gov/pubmed/12600311

Vale, R. D., Funatsu, T., Pierce, D. W., Romberg, L., Harada, Y., & Yanagida, T. (1996). Direct observation of single kinesin molecules moving along microtubules. *Nature, 380*(6573), 451-453. doi:10.1038/380451a0

Vale, R. D., Reese, T. S., & Sheetz, M. P. (1985). Identification of a novel force-generating protein, kinesin, involved in microtubule-based motility. *Cell, 42*(1), 39-50. Retrieved from https://www.ncbi.nlm.nih.gov/pubmed/3926325

Vance, C., Rogelj, B., Hortobagyi, T., De Vos, K. J., Nishimura, A. L., Sreedharan, J., . . . Shaw, C. E. (2009). Mutations in FUS, an RNA processing protein, cause familial amyotrophic lateral sclerosis type 6. *Science, 323*(5918), 1208-1211. doi:10.1126/science.1165942

Weedon, M. N., Hastings, R., Caswell, R., Xie, W., Paszkiewicz, K., Antoniadi, T., . . . Ellard, S. (2011). Exome sequencing identifies a DYNC1H1 mutation in a large pedigree with dominant axonal Charcot-Marie-Tooth disease. *Am J Hum Genet, 89*(2), 308-312. doi:10.1016/j.ajhg.2011.07.002

Xia, C. H., Roberts, E. A., Her, L. S., Liu, X., Williams, D. S., Cleveland, D. W., & Goldstein, L. S. (2003). Abnormal neurofilament transport caused by targeted disruption of neuronal kinesin heavy chain KIF5A. *J Cell Biol, 161*(1), 55-66. doi:10.1083/jcb.200301026

Zhao, C., Takita, J., Tanaka, Y., Setou, M., Nakagawa, T., Takeda, S., . . . Hirokawa, N. (2001). Charcot-Marie-Tooth disease type 2A caused by mutation in a microtubule motor KIF1Bbeta. *Cell, 105*(5), 587-597. Retrieved from https://www.ncbi.nlm.nih.gov/pubmed/11389829

Figure legends

Figure 1 Cellular distribution of ALS-associated KIF5A mutant

(A) Schematic drawing of ALS mutations in KIF5A. ALS-associated KIF5A mutations (asterisks) are often found in introns around exon 27 and commonly induces missplicing of exon 27 and frameshift. Amino acid sequences show C-terminal sequences of wild type KIF5A (Black font) and KIF5A(Δexon27) (Purple font).

(B) Schematic drawing showing mScarlet-fused wild type KIF5A (mSca::KIF5A) and mScarlet-fused mutant KIF5A(mSca:: KIF5A(Δexon27)) used in Figure 1.

(C-E) mSca::KIF5A and mSca::KIF5A(Δexon27) were expressed in CAD cells and analyzed by fluorescent microscopy. (C and D) Representative images showing the localization of mSca::KIF5A (C) and mSca::KIF5A KIF5A(Δexon27) (D). Bars, 10 μm. (E) The cells were classified by the distribution of mScarlet signals into two categories: no aggregations (light gray) and with aggregation (dark gray), and the number of cells in each category was counted. n= 91 mScarlet-expressed cells, 92 KIF5A(wt)-expressed cells, 88 KIF5A(Δexon27) -expressed cells and 73 KIF5B-expressed cells. Chi-square test with Bonferroni correction. ns, Adjusted P Value > 0.05 and statistically not significant. *, Adjusted P Value < 0.05. **, Adjusted P Value < 0.01, ****

Adjusted P Value < 0.0001.

Figure 2 Co-aggregation of ALS-associated KIF5A

mScarlet fused KIF5A or KIF5A(Δexon27) was co-expressed with EGFP fused proteins in CAD cells.

(A and B) Representative images showing mSca::KIF5A (A) and EGFP::KIF5A (B) co-expressed cells.

When mSca::KIF5A did not form aggregates, EGFP::KIF5B did not co-aggregate in the same cell.

(C and D) Representative images showing mSca:: KIF5A(Δexon27) (C) and EGFP::KIF5A (D) co-expressed cells. Note that EGFP::KIF5A co-aggregated with mSca:: KIF5A(Δexon27). 100% cells (85/85) showed co-aggregations.

(E and F) Representative images showing mSca::KIF5A (E) and EGFP::KIF5B (F) co-expressed cells. When mSca::KIF5A did not form aggregates, EGFP::KIF5B did not co-aggregate as well.

(G and H) Representative images showing mSca:: KIF5A(Δexon27) and EGFP::KIF5B co-expressed cells. Note that EGFP::KIF5B co-aggregated with mSca:: KIF5A(Δexon27). 100 % cells (82/82) showed co-aggregation.

(I and J) Representative images showing mSca:: KIF5A(Δexon27) and EGFP co-expressed cells. Even if mSca:: KIF5A(Δexon27) formed aggregates in the cytoplasm, no GFP aggregations were observed. 0/54 cells showed co-aggregation.

Bars, 10 μm.

Figure 3 Purification of KIF5A and KIF5A(Δexon27)

mScarlet was added to the C-terminal of either KIF5A (KIF5A::mSca) or KIF5A(Δexon27) (KIF5A(Δexon27)::mSca). Recombinant proteins were expressed in sf9 cells and purified.

(A and B) Normalized size exclusion chromatograms for KIF5A::mSca and KIF5A(Δexon27)::mSca (A) and KIF5A::mSca-KLC1 and KIF5A(Δexon27)::mSca-KLC1 (B). Yellow shaded area shows the void volume of the column corresponding to potential aggregates, red shaded area shows the fractions corresponding to oligomers, and blue shaded area shows the fractions corresponding to KIF5A dimer or KIF5A-KLC1 tetramer. Wild type protein from the blue shaded fraction and Δexon27 protein from the red shaded fraction were used for TIRF assays, respectively.

(C) Coomassie blue stained gel showing the purified KIF5A::mSca, KIF5A(Δexon27)::mSca, KIF5A::mSca-KLC1, KIF5A(Δexon27)::mSca-KLC1.

Figure 4 Motility of ALS-associated KIF5A on microtubules

The motility of 10 nM KIF5A::mSca, 10 nM KIF5A(Δexon27)::mSca, 10 nM KIF5A::mSca-KLC1 complex and 10 nM KIF5A(Δexon27)::mSca-KLC1 complex on microtubules in the presence of 2

mM ATP were observed by TIRF microscopy.

(A) Representative TIRF images of KIF5A (magenta) and microtubules (cyan). Note that KIF5A(Δexon27)::mSca and KIF5A(Δexon27)::mSca-KLC1 bound to microtubule more frequently than KIF5A::mSca and KIF5A::mSca-KLC1. Bars, 10 µm.

(B) Representative kymographs of KIF5A::mSca, KIF5A(Δexon27)::mSca, KIF5A::mSca-KLC1 complex and KIF5A(Δexon27)::mSca-KLC1 complex. Scale bars are 10 s (vertical) and 10 µm (horizontal).

(C) Dot plots showing the landing rate of KIF5A::mSca (wt), KIF5A(Δexon27)::mSca (Δexon27), KIF5A::mSca-KLC1 complex (wt+KLC1) and KIF5A(Δexon27)::mSca-KLC1 complex (Δexon27+KLC1). The number of KIF5A that bound to microtubules was counted and adjusted by the time window, microtubule length and concentration. Each dot shows one datum. N = 20 kymographs from each sample. Brown-Forsythe and Welch ANOVA followed by Dunnett's multiple comparisons test. ***, Adjusted P Value < 0.001. ****, Adjusted P Value < 0.0001.

(D) Dot plots showing the run length of KIF5A(Δexon27)::mSca (Δexon27) and KIF5A(Δexon27)::mSca-KLC1 complex (Δexon27+KLC1). n = 202 (Δexon27) and 201 (Δexon27+KLC1). Mann-Whitney test. ns, Adjusted P Value > 0.05 and statistically not significant

(E and F) Gaussian fit and histogram showing the velocity of KIF5A(Δexon27) and KIF5A(Δexon27)::mSca-KLC1 complex. 377 ± 107 nm/sec (KIF5A(Δexon27)) and 378 ± 111nm/sec (KIF5A(Δexon27)-KLC1). Mean ± Standard deviation obtained from best-fit values. n = 349, 337, respectively. The velocity of KIF5A(Δexon27) was not affected by KLC1. Note that enough number of samples could not be collected in the case of KIF5A(wt)::mSca and KIF5A(wt)::mSca-KLC1.

Figure 5 Aggregation formation *in vitro*

1 µM of purified mScarlet or KIF5A(Δexon27)::mSca were incubated at 37°C.

(A) Turbidity of the solution. Optical density of samples measured at a wavelength of 600 nm (OD600) was measured and plotted at indicated time points. Results from three independent experiments are shown for KIF5A(Δexon27)::mSca.

(B) After 24 hours incubation, samples were centrifuged at 18000 g for 10 min and pellet was observed. Note that protein pellet is induced in KIF5A(Δexon27)::mSca sample while no pellet was observed in purified mScarlet.

Figure 6 Neuronal toxicity in *C. elegans*

Human KIF5A or KIF5A(Δexon27) were expressed in a worm strain expressing GFP in mechanosensory neurons.

(A and B) Morphology of PVM and PLM mechanosensory neurons. Schematic drawing of PVM and

PLM neurons (A) and a representative image of PVM and PLM neurons visualized by GFP expressed under the *mec-7* promoter (*Pmec-7*).

(C-E) Representative images showing *Kif5a*-expressing mechanosensory neurons (C) and *Kif5a(Δexon27)*-expressing neurons (D and E). Some worms have degenerated PLM neuron (D) while some worms show neuronal loss. Bars, 100 μm.

(F) Worm phenotypes were classified by the morphology of mechanosensory neurons into two categories: normal morphology (light gray) and abnormal morphology (dark gray), and the number of worms in each category was counted. n= 87 (control strain), 68 (KIF5A(wt)-expressed strain #1), 75 (KIF5A(wt)-expressed strain #2), 73 (KIF5A(Δexon27)-expressed strain #1) and 79 (KIF5A(Δexon27)-expressed strain #2) worms. Chi-square test with Bonferroni correction. ns, Adjusted P Value > 0.05 and statistically not significant, ****, Adjusted P Value < 0.0001. Compared with the control strain.

A

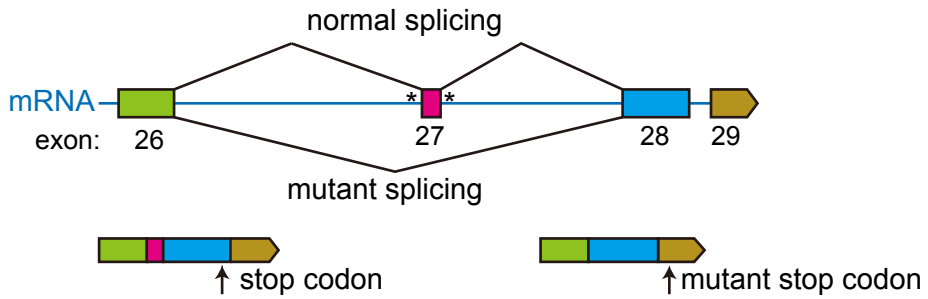

MDNGNATDINDNRSDLPCGYEAEDQAKLFPLHQETAAS*

MDNGVTCRVAMRLRTRPSFSLSTKRQQPANLPHPRLHTCTFSF*

B

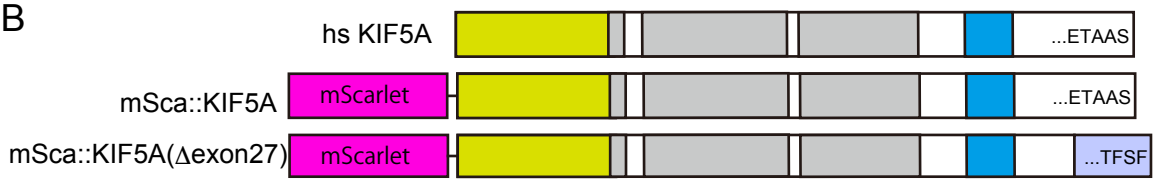

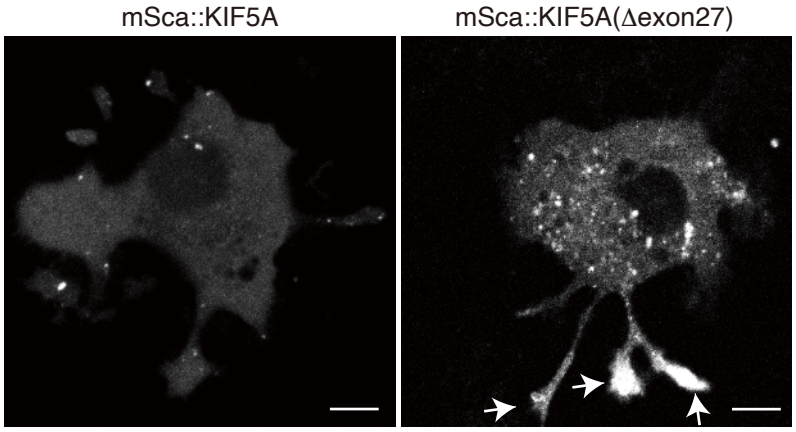

E

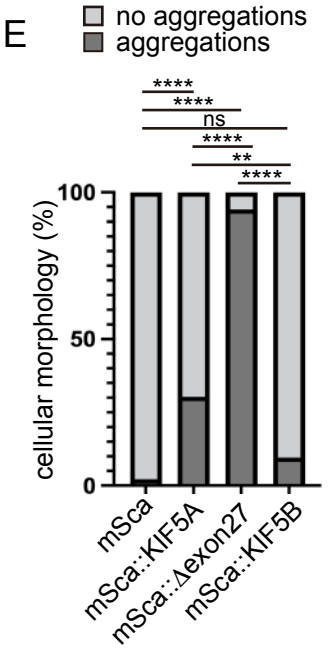

Figure 1

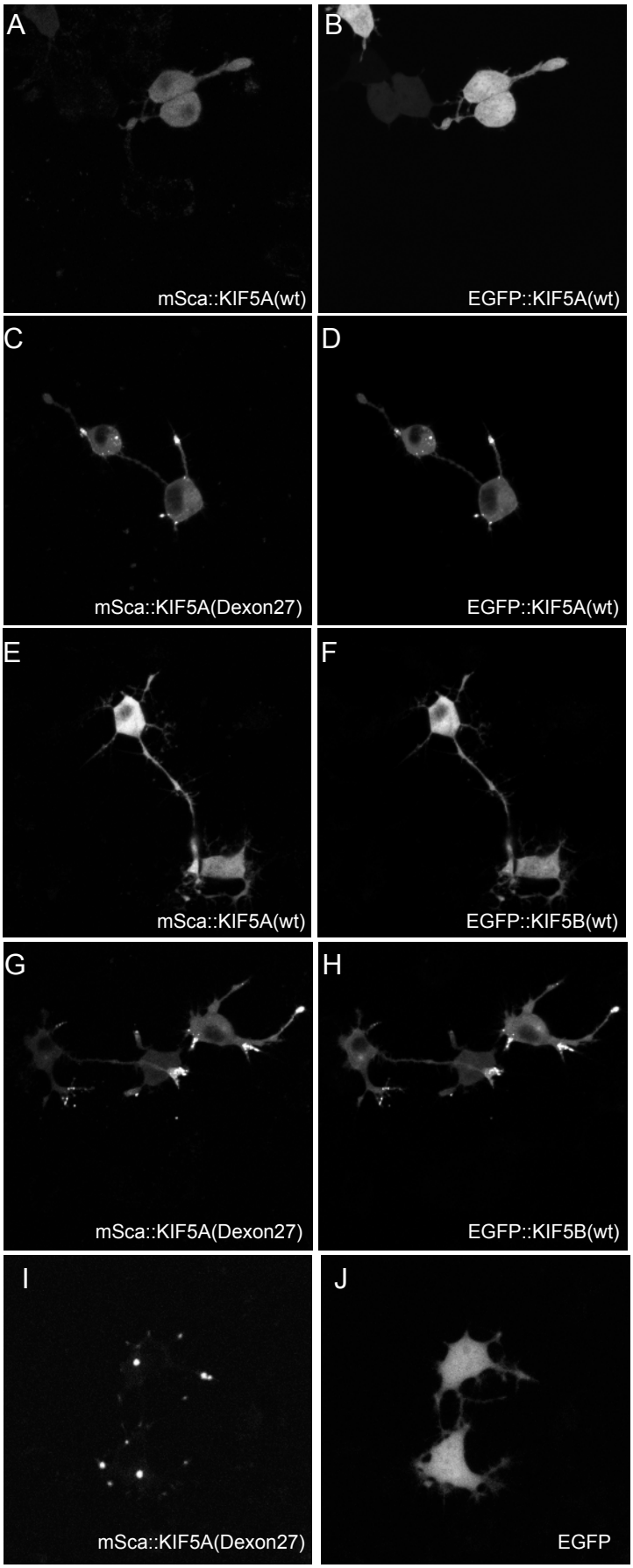
A
mSca::KIF5A(wt)
B
EGFP::KIF5A(wt)
C
mSca::KIF5A(Dexon27)
D
EGFP::KIF5A(wt)
E
mSca::KIF5A(wt)
F
EGFP::KIF5B(wt)
G
mSca::KIF5A(Dexon27)
H
EGFP::KIF5B(wt)
I
mSca::KIF5A(Dexon27)
J
EGFP

Figure 2

A

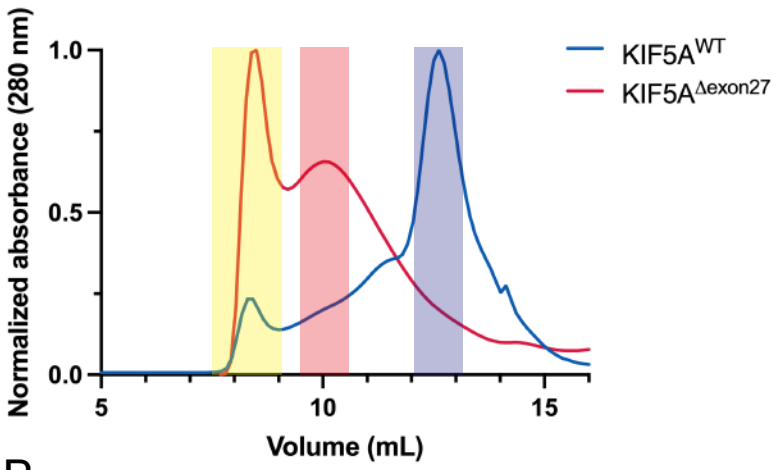
Normalized absorbance (280 nm)
1.0
0.5
0.0
5
10
15
Volume (mL)
KIF5A^WT
KIF5A^Δexon27

B

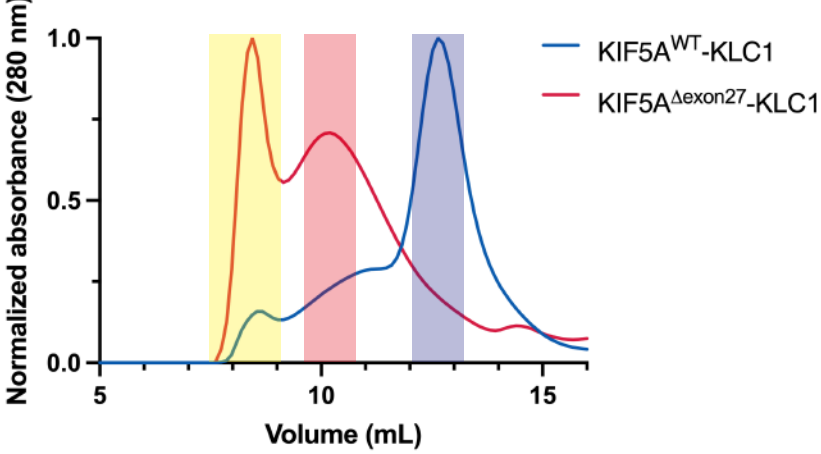
Normalized absorbance (280 nm)
1.0
0.5
0.0
5
10
15
Volume (mL)
KIF5A^WT-KLC1
KIF5A^Δexon27-KLC1

C

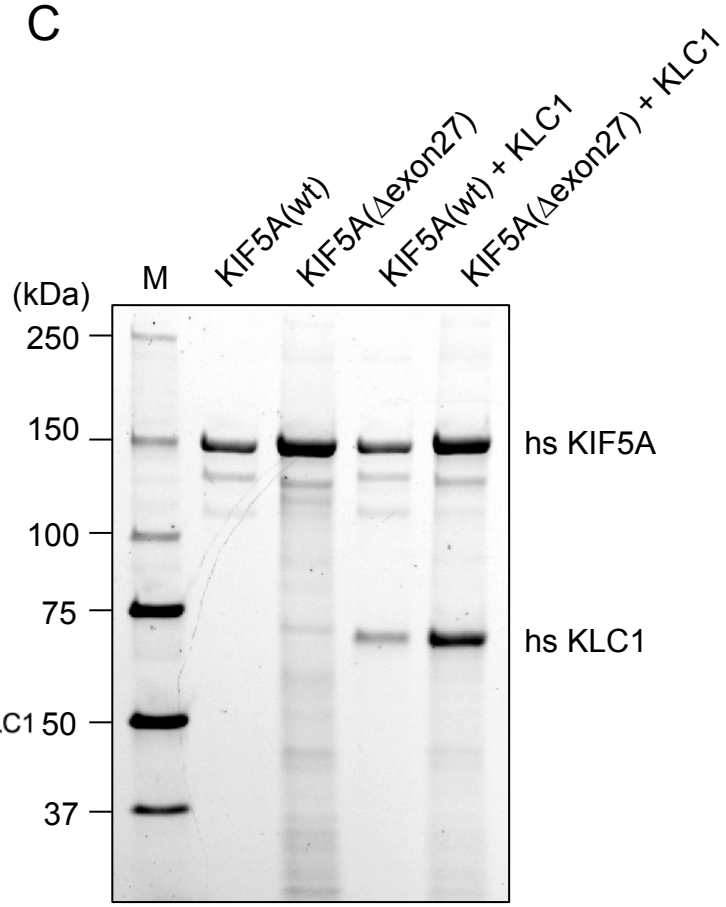
M
KIF5A(wt)
KIF5A(Δexon27)
KIF5A(wt) + KLC1
KIF5A(Δexon27) + KLC1
(kDa)
250
150
100
75
50
37
hs KIF5A
hs KLC1

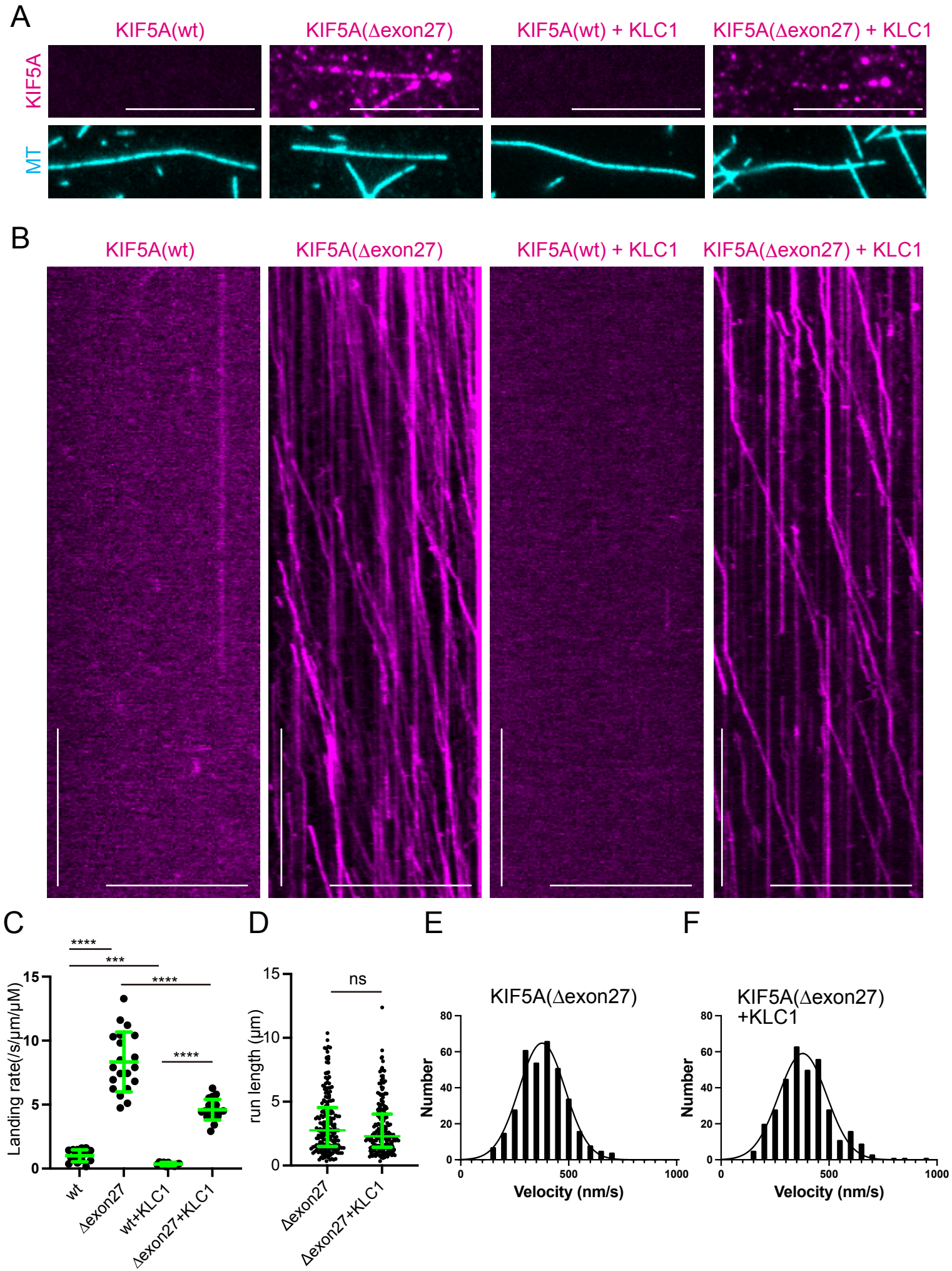
A
KIF5A(wt)
KIF5A(Δexon27)
KIF5A(wt) + KLC1
KIF5A(Δexon27) + KLC1
KIF5A
MT
B
KIF5A(wt)
KIF5A(Δexon27)
KIF5A(wt) + KLC1
KIF5A(Δexon27) + KLC1
C
Landing rate(/s/μm/μM)
****
***
****
****
wt
Δexon27
wt+KLC1
Δexon27+KLC1
D
run length (μm)
ns
Δexon27
Δexon27+KLC1
E
KIF5A(Δexon27)
Number
Velocity (nm/s)
F
KIF5A(Δexon27)
+KLC1
Number
Velocity (nm/s)

A

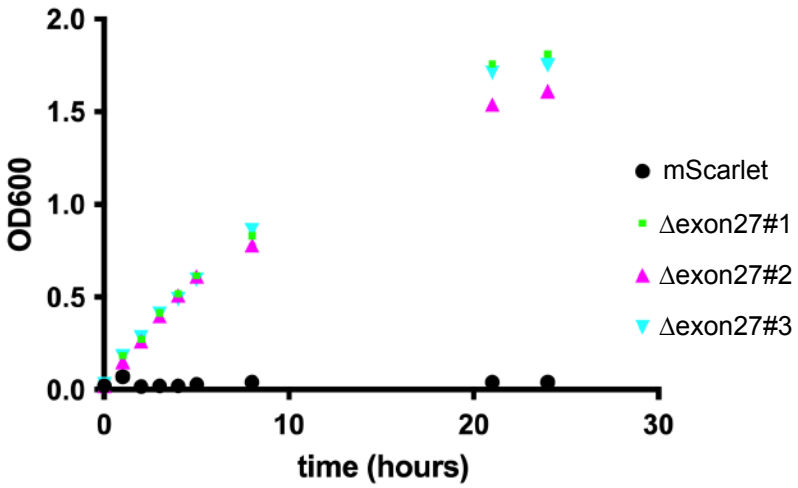
2.0
1.5
1.0
0.5
0.0
OD600
0
10
20
30
time (hours)
mScarlet
Δexon27#1
Δexon27#2
Δexon27#3

B

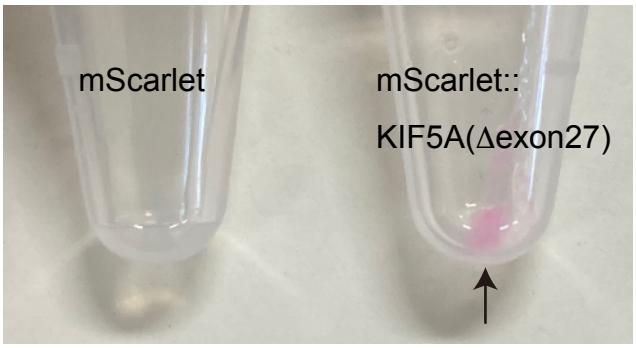
mScarlet
mScarlet::
KIF5A(Δexon27)

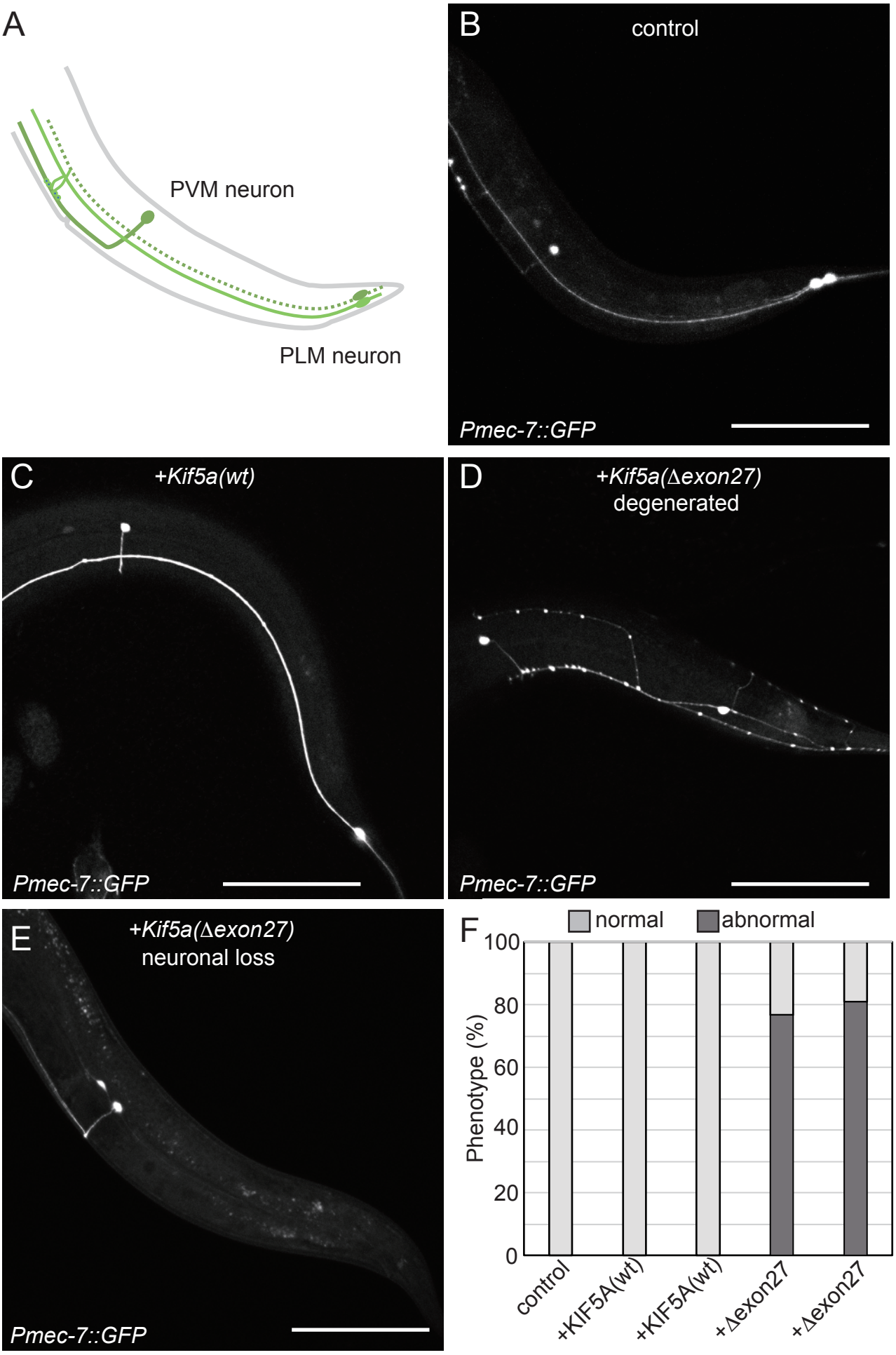
A
PVM neuron
PLM neuron
B
control
Pmec-7::GFP
C
+Kif5a(wt)
Pmec-7::GFP
D
+Kif5a(Δexon27)
degenerated
Pmec-7::GFP
E
+Kif5a(Δexon27)
neuronal loss
Pmec-7::GFP
F
normal
abnormal
Phenotype (%)
100
80
60
40
20
0
control
+KIF5A(wt)
+KIF5A(wt)
+Δexon27
+Δexon27

Figure 6